Geophysical Journal International

Geophys. J. Int. (2020) **222,** 225–230
Advance Access publication 2020 April 11
GJI Geodynamics and tectonics

doi: 10.1093/gji/ggaa158

EXPRESS LETTER

Composite damage zones in the subsurface

Zonghu Liao [1], Wei Li,[1] Huayao Zou,[1] Fang Hao,[2] Kurt J. Marfurt[3] and Ze'ev Reches [3]

[1] *State Key Laboratory of Petroleum Resources and Prospecting, College of Geosciences, China University of Petroleum (Beijing), Beijing* 102249, *China. E-mail: Zonghuliao@163.com*
[2] *School of Geosciences, China University of Petroleum, Qingdao, Shandong* 266555, *China*
[3] *School of Geology and Geophysics, University of Oklahoma, Norman, OK* 73072, *USA*

Accepted 2020 March 30. Received 2020 March 25; in original form 2019 November 4

SUMMARY

The cumulative displacement by multiple slip events along faults may generate composite damage zones (CDZ) of increasing width, and could modify the hydraulic and mechanical properties of the faults. The internal architecture and fracture distribution within CDZs at the subsurface are analysed here by using seismic attributes of variance, curvature and dip-azimuth of the 3-D seismic reflection data from tight sandstone reservoirs in northeast Sichuan, China. The analysed faults intersect the reservoir within a depth range of 2.4–3.0 km. The damage intensity mapping revealed multiple CDZs with thicknesses approaching 1 km along faults ranging 3–15 km in length, and up to 1000 m of cumulative slip. The identification of numerous fault cores and associate damage zones led us to define three classes of CDZs: banded shape, box shape and dome shape. The mechanical strength contrasts and distortion of fault cores suggest potential weakening and strengthening (healing) mechanisms for formation of CDZs that can be extended to faulting processes and earthquake simulations.

Key words: Asia; Computational seismology; Dynamics and mechanics of faulting.

1 INTRODUCTION

Faulting is typically preceded by fragmentation and slip along microfractures that eventually coalesce to form a macroscopic fault zone (Reches & Lockner 1994; Scholz 2002; Savage & Brodsky 2011). The fragmented and fractured rock bodies form a wide damage zone with a fault core of localized slip as recognized in many laboratory experiments, field exposures and subsurface analyses (Fig. 1; Billi *et al.* 2003; Faulkner *et al.* 2003). Renewed deformation at the proximity of an existing fault zone can occur in two general ways: (1) reactivation of fault with slip along the existing fault core, a process that reflects long-term fault weakening, or (2) slip away from the fault core, within the damage zone or at the contact with the intact host rock (Fig. 1a). This process widens the deformed zone to develop a complex structure that can be described as composite damage zone (CDZ; Fig. 1B; Caine *et al.* 1996; Faulkner *et al.* 2003; Johansen *et al.* 2005). Observations of exposed CDZs reveal multiple fault cores of localized slip with associated damage zones that can be hundreds of metres wide (e.g. Faulkner *et al.* 2003; Di Toro & Pennacchioni 2005). Typically, the intensity of fracture damage is highest close to the fault core and diminishes outwards (e.g. Sagy *et al.* 2001; Billi *et al.* 2003; Faulkner *et al.* 2010; Savage & Brodsky 2011). The existence and geometry of composite damage zones strongly affect the hydrological and mechanical properties of the local crust. Notably, CDZs can control the migration, accumulation and leakage of subsurface fluids in hydrocarbon reservoirs, and the strength of the surrounding blocks (Lyakhovsky & Ben-Zion 2009; Faulkner *et al.* 2010; Heesakkers *et al.* 2011). Further, a damage zone could control the style of seismic slip during an earthquake. For example, in their evaluation of the seismic hazard in California, Field *et al.* (2014) considered existing fault zones as polygons that may integrate simple slip surfaces and a system of braided faults, a structure that fits the characteristics of composite damage zones.

We focus here on the analysis of CDZs in the subsurface, including defining their internal structure and discussion of their possible evolution. Fractures and rock damage are almost invisible on typical seismic profiles. Therefore, previous studies used indirect methods to detect subsurface CDZs, including synthetic wave modelling (Peng *et al.* 2003), analysis of natural variations of seismicity rate (Powers & Jordan 2010), earthquake locations (Valoroso *et al.* 2014) and seismic velocity distribution (Ben-Zion & Sammis 2003). Here, we directly map CDZs by using the seismic attributes (variance, curvature and dip-azimuth) of a 3-D seismic survey that allows us to characterize fault structure and deformation patterns at a resolution of about 50 m (Chopra & Marfurt 2007; Iacopini & Butler 2011; Liao *et al.* 2018). Our analysis utilizes surveys in the northeast Sichuan Basin, China, which cover an area of about 225 km^2.

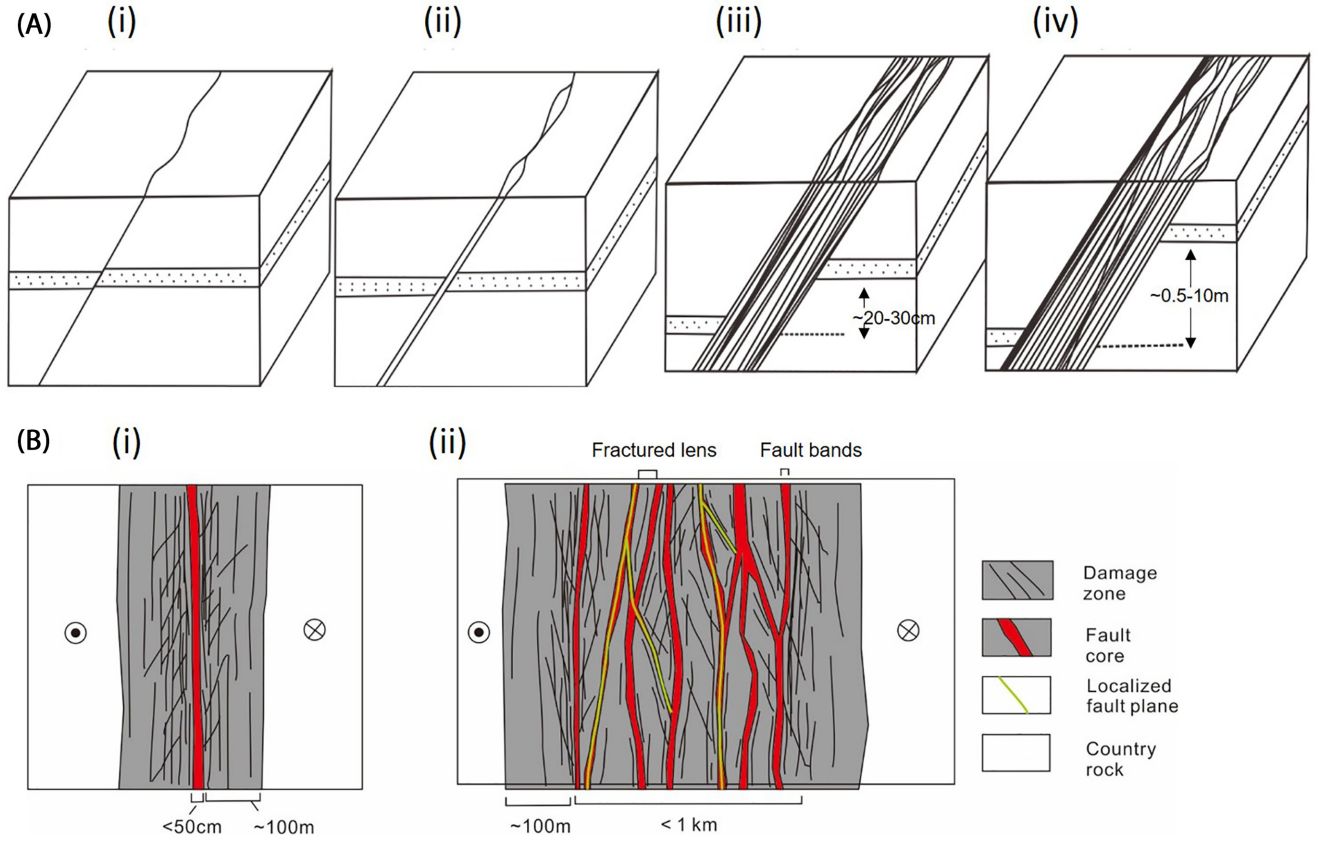

Figure 1. Conceptual models of the evolution of a CDZ in field exposures. (a) Sequential development of a CDZ in porous sandstone, Utah; evolution from a single damage band (i) through zones of deformation bands (ii, iii) to a fault with multiple bands of CDZs (iv) (after Aydin & Johnson 1978). (b) Evolution of a strike-slip fault from a single fault zone (i) to a complex CDZ (ii); based on structural analysis of the Carboneras fault, SE Spain (after Faulkner *et al.* 2003).

2 COMPOSIT DAMAGE ZONES IN SICHUAN BASIN

2.1 Tectonic setting

The analysis utilizes 3-D seismic data from the Tongnanba anticline in the northeast of the Sichuan Basin, China. The anticline is bounded by the Micangshan thrust system in the north, the Dabashan thrust fold belt in the east (Fig. 2), and the Longmenshan fault and fold belt in the far west. The Tongnanba anticline was created in two major tectonic stages (Li *et al.* 2016). First, NW–SE compression of the Xujiahe Formation in the Jurassic formed the 100-km-long, 8-km-wide Tongnanba anticline (Fig. 2). Second, NE–SW compression beginning in the Neogene and driven by the Himalayan Orogenic broke and deformed the Tongnanba anticline along a system of reverse faults (Fig. 2). The cumulative offset of the fault system is estimated to be 3.0 km (ranging from 100 to 1000 m for each fault). The present analysis focuses on the structure and evolution of the reverse faults and their associated damage zones. These faults intersect the principal gas-bearing Triassic Xujiahe sandstone within a depth range of 2.4–3.0 km, and the fault damage zones possibly control the high production of Xujiahe sandstone.

2.2 Seismic attributes

We analysed the structure of the reverse faults using a 3-D seismic reflection data set of an area of about 225 km^2, which was provided by Sinopec China. The data set was collected at main frequency of 60 Hz. Key acquisition parameters include 50 m × 50 m common depth points, 240 channels with 40 m spacing, shot interval of 160 m, 30-fold stacking, combined geophone, 18–20 m well-depth and 12–14 kg of explosive, high-density shaped seismic source, 8 s recording with 12 dB pre-amplifier gain and sampling rate of 1 ms (Teng 2005; Liao *et al.* 2020). The data set indicates increased impedance as positive amplitude, with Kirchhoff pre-stack time migration. To identify the subsurface structure and characterize the damage zones, we computed a set of four volumetric seismic attributes (Fig. 3): reflection amplitude, dip-azimuth, curvature and seismic variance.

The 'dip-azimuth' attribute (Marfurt 2006) shows the local dip-direction of the layers of the Xujiahe Formation in the time-migrated seismic profiles (Fig. 3b). This map reveals two superposed structural features (Fig. 3b): first, the Tongnanba anticline, with NW limb dipping towards 335°–345°, and the SE limb dipping to southeast, 90°–120°. Second, three large zones, with trend marked by a thin dotted line, of local dipping reflector towards 50°–80°, that cut across the anticline. We computed the most-positive curvature (K1, red) for anticlinal flexures and most-negative curvature (K2, blue) for synclinal flexures, which together reveal flexures related to the reverse faults (Chopra & Marfurt 2007). The curvature map (Fig. 3c) reveals: (1) two major fold zones (yellow arrows) striking 335°–345°; (2) each fold zone is composed of red anticlines in west and blue synclines in east; (3) several small northeast-trending lineaments cross-cut the top of the two major folds. The wells with high gas production, M101 and M103, located at the anticline crest (Fig. 3e), are close to the central fold zone.

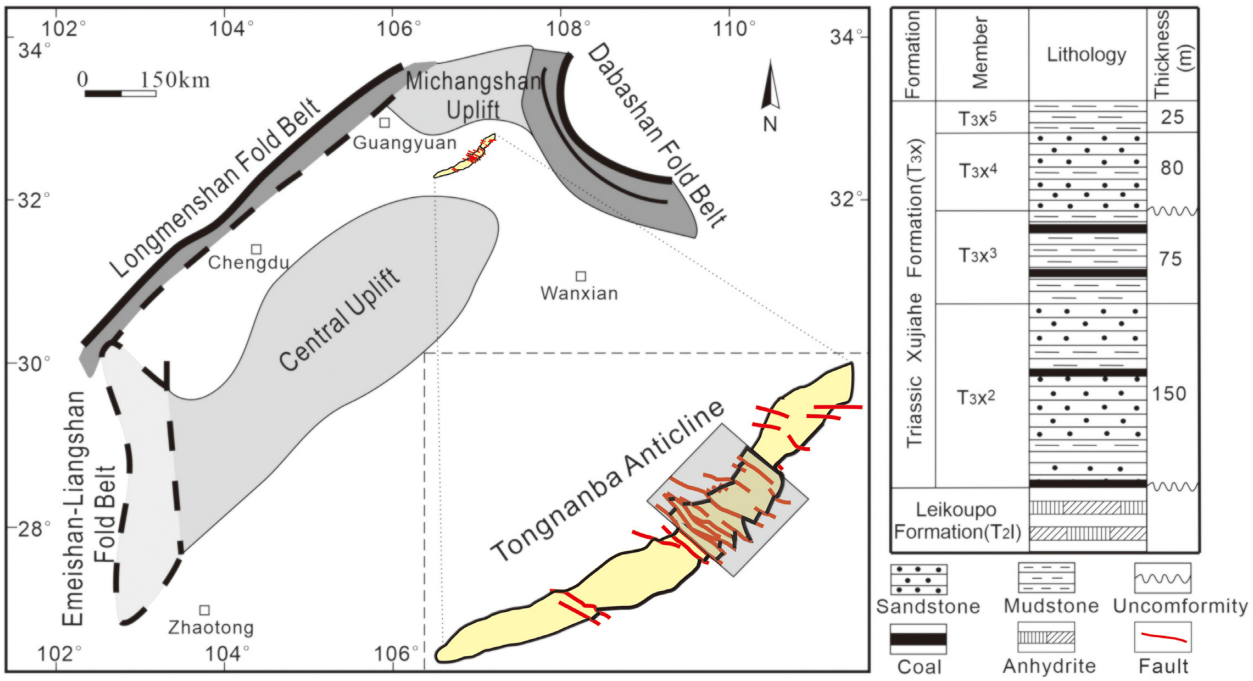

Figure 2. Structural setting of study area in northeast Sichuan Basin, China, showing the general boundaries of the basin, and the Tongnanba anticline striking northeast (yellow in the inset). The analysed seismic data cover the shaded area, and the analysed reverse faults are marked red. Right: a simplified stratigraphic section of the Xujiahe formation.

Finally, to identify the damage zones, we mapped the variance attribute (Fig. 3d) that is a measure of similarity between waveforms or traces in 3-D seismic volumes. This attribute is designed to emphasize discontinuous events of faults (Chopra & Marfurt 2007). The 3-D variance along the reflector dip reveals (Fig. 3d) that the Tongnaba anticline is interrupted by three long high variance lineaments accompanied by three shorter lineaments that strike 335°–345°, parallel to the Dabashan thrust fold belt, about 60 km northeast of the mapped area (Fig. 2). We refer to this system as the northwest-trending reverse faults.

Based on the above three seismic attributes (Figs 3b–d), we identify six major reverse faults with strike numbered F1–F6 (Fig. 3d). The curvature and dip-azimuth attributes indicate that F3 and F6 are associated with secondary anticlinal and synclinal flexures. The other faults display relatively smaller deformation intensity.

2.3 Composite damage zones

The seismic disturbance zones detected in the present analysis are regarded as CDZs associated with the reverse faults described above (Chopra & Marfurt 2007; Iacopini & Butler 2011; Liao *et al.* 2018). The seismic variance levels in 3-D-seismic analysis indicate the intensity of structural disturbance and discontinuities, which we interpret as three levels of damage intensity according to the variance values. The zone with high variance values is considered as a fault core, the intermediate level zone is regarded as the damage zone and the low variance zone is interpreted as protolith zone. Liao *et al.* (2018) showed that the variance zonation in the subsurface matches field observations (Sagy *et al.* 2001; Mitchell & Faulkner 2009; Savage & Brodsky 2011). Superposition of multiple faults is expected to generate CDZs (Chester *et al.* 2004; Savage & Brodsky 2011).

We prepared 18 vertical profiles of the seismic variance that are arranged in four sections across faults F3 and F4 (yellow lines in Fig. 3e). The profiles in each section display a similar distribution of the seismic variance that we generalized as the characteristic damage zones (Figs 4d, f and h). These sections reveal four styles of damage zones:

(1) Pulse section (F4-b in Fig. 4a) is a typical damage zone of a single fault (Liao *et al.* 2018) with a central zone of high variance, >0.4, (pink in Fig. 4a), and two zones of intermediate variance, 0.1–0.4, that decay exponentially to the background variance, 0–0.1 (Fig. 4b). Schematic section is shown in Fig. 4(c).

(2) Banded section of ∼900 m width (F3–2b in Fig. 4d) with three large fault cores (high variance) that are separated by corresponding damage zones; note three smaller cores on the left and two smaller ones on the right. Schematic section is shown in Fig. 4(e).

(3) Box section of ∼500 m width (F4 in Fig. 4f) with multiple anastomosing fault cores and damage zones without distinct variance pulses of individual cores. Schematic section is shown in Fig. 4(g).

(4) Dome section of ∼1200 m width (F3–1 in Fig. 4h) with multiple cores and damage zones that gradually decay in variance intensity from the central core. Schematic section is shown in Fig. 4(i).

3 DISCUSSION: EVOLUTION OF COMPOSITE DAMAGE ZONES

Increasing displacement along a fault system may generate new faults with separate cores and damage zones that form a CDZ, as described above and elsewhere (Aydin & Johnson 1978; Faulkner *et al.* 2003). The formation of a CDZ is somewhat puzzling because it is expected that an existing fault zone is the weakest regional feature, and continuous deformation should localize along it. Indeed, this style prevails along many faults with slip localization within zones of ≤1 m thickness along faults of tens of km, for example, the San-Andreas fault, or the Glarus thrust (Badertscher & Burkhard

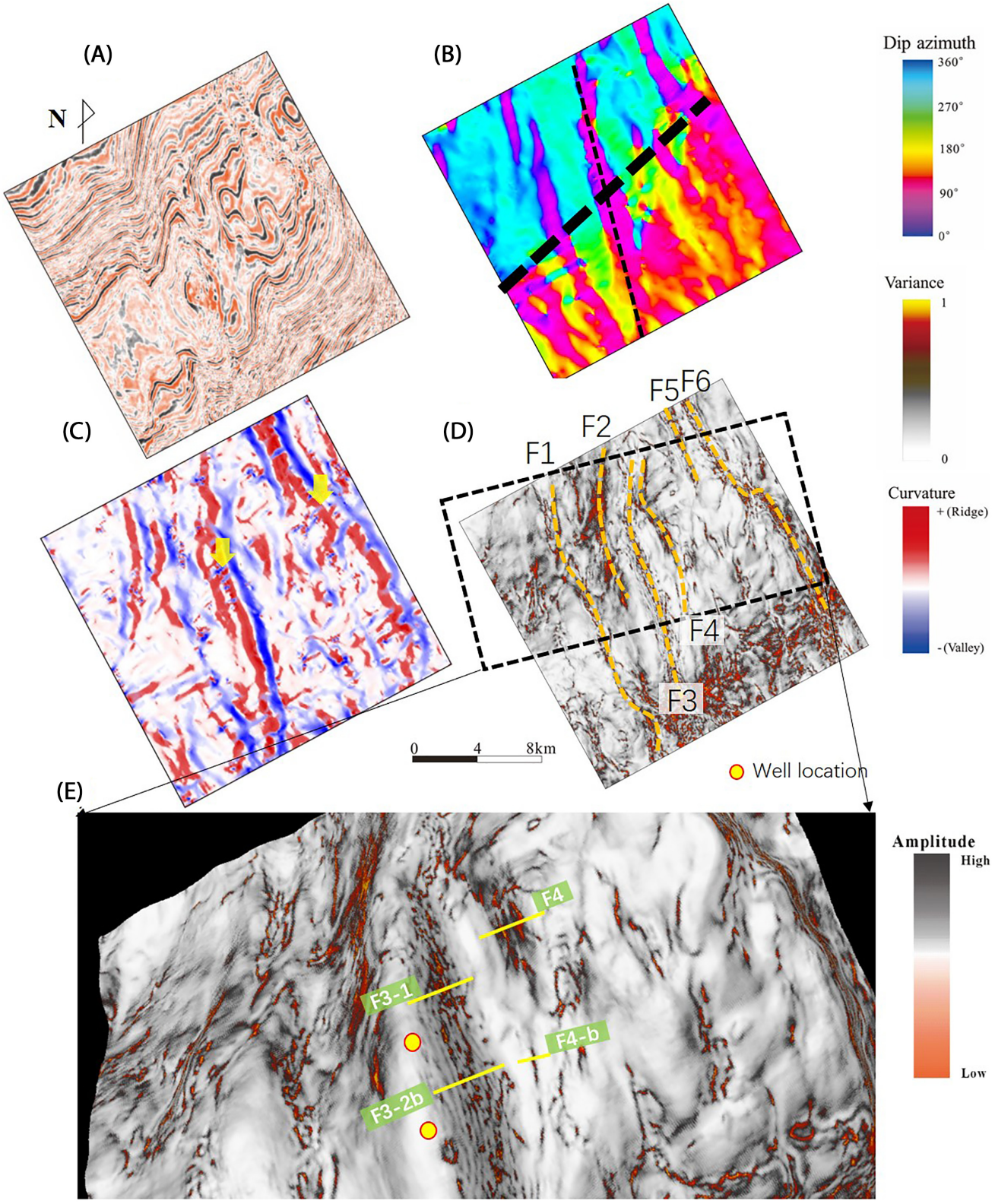

Figure 3. Maps of calculated attributes of the 3-D seismic survey (shaded area in Fig. 2). (a) Seismic amplitude of the Xujiahe sandstone. (b) Dip-azimuth attribute with general axis of the anticline (thick black line). (c) Curvature attribute (see the legend). (d) Variance attribute with marked trends of the interpreted faults (yellow) (see the text). (e) Zoom-in of the rectangle in (d) displaying the locations of the CDZ profiles shown in Fig. 4 (yellow lines) and location of wells M101 and M103.

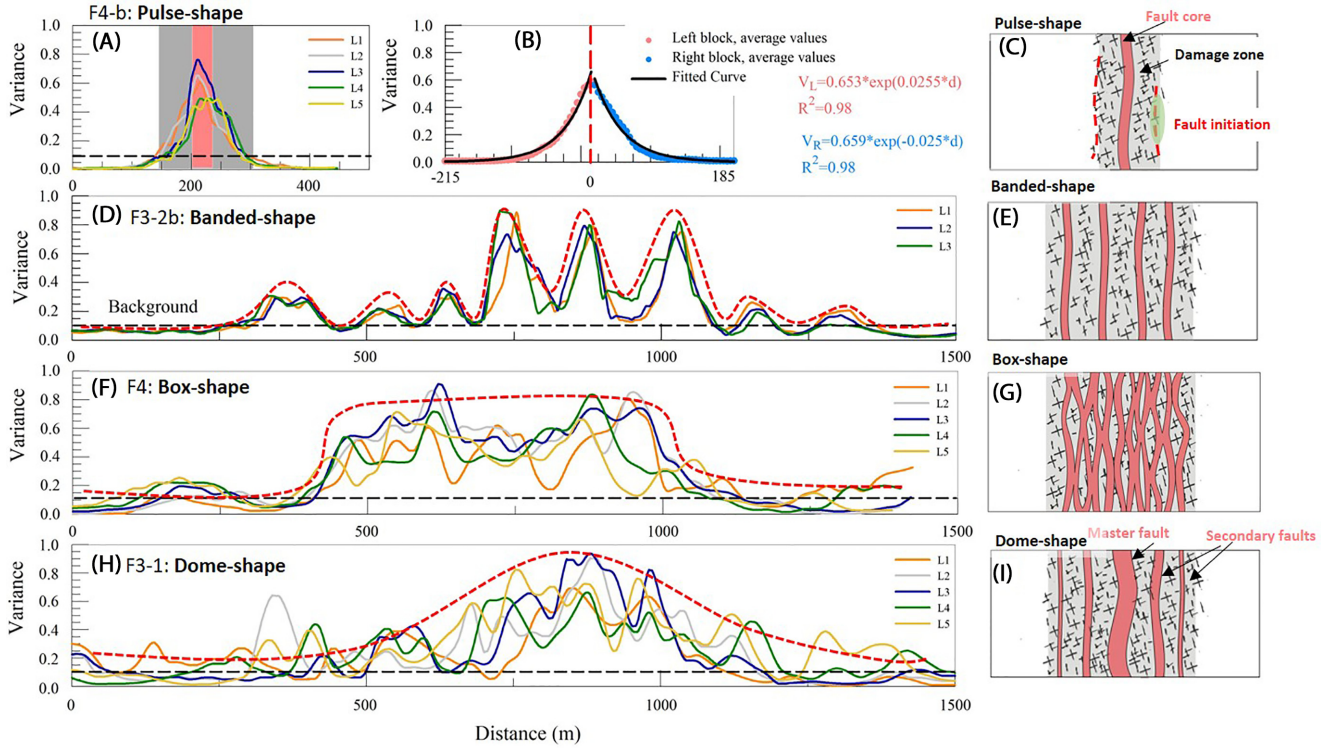

Figure 4. Profiles of the seismic variance values across the CDZs associated with the reverse faults at the Xujiahe tight sandstone level; profiles' locations in Fig. 3(e); variance values above background are interpreted as damage zones. (a) Single core damage zone along Fault 4-b. (b) Variance exponential decay away from the fault core interpreted as the damage zone. (c) Existing individual fault zone with its damage zone and potential site for renewed slip. (d) Banded-shape CDZ with approximately equal-size fault cores parallel/sub-parallel as seen in three profiles across Fault 3–2b, and idealized shape in (e). (f) Box-shape CDZ with multiple, anastomosing fault cores as seen in five profiles across Fault 4, and idealized shape in (g). (h) Dome-shape CDZ with one dominating fault core and a few secondary ones as seen in five profiles across Fault 3–1, with idealized shape in (i). Note the generalized damage intensity curves (dashed red) in all three classes of composite damage zones (d, f and h).

2000; Chester *et al.* 2004). This localization indicates that the fault maintains low static strength relative to the host blocks (Lockner *et al.* 2011). On the other hand, CDZs will form when the existing fault is stronger than the surrounding rock mass, and three main settings could lead to this situation:

(i) A CDZ can develop if the slip along a fault produces fault core that is stronger than the host rock. Aydin & Johnson (1978) investigated the evolution of fault zones in porous sandstone layers. They recognized a hierarchy of three structural levels of shear structures: deformation bands of a few mm slip and ∼1 mm thickness, zones of deformation bands that are composed of tens of subparallel deformation bands and slip surfaces of localized slip on the order of metres (Fig. 1a). Aydin & Johnson (1978) attributed this evolution to strain hardening of the deformation bands due to the reduction of the sandstone porosity due to grain crushing during shear. Another example was presented in Di Toro & Pennacchioni (2005) study of the Gole Larghe fault in the Alps. The continuous shear along Gole Larghe fault zone formed hundreds of new segments in a CDZ (Di Toro & Pennacchioni 2005) because the shear strength of the glassy segments was higher than the strength of the joints in the damaged host rock.

(ii) A CDZ can form due to healing and strengthening of a fault zone during periods of no-slip as demonstrated experimentally (e.g. Muhuri *et al.* 2003) or due to a higher mechanical efficiency along boundaries between damaged and undamaged rocks during the slip period (Ben-Zion & Andrews 1998). Heesakkers *et al.* (2011) map the rupture zone of an M2.2 earthquake that reactivated an ancient fault network in Tautona Mine, South Africa. They found that the slip was systematically localized along the contacts between the ancient fault core and the damaged quartzitic host rocks, which is controlled by the contrast of mechanical properties between the cataclasite and the host rocks. Multiple occurrences of this process could lead to a widening of the damage zone and formation of a CDZ.

(iii) A third mechanism is related to structural complexity. Segmented, non-planar faults (Caine *et al.* 1996; Faulkner *et al.* 2010), which form by inherent randomness of fracturing or due to temporal stress rotation, are stronger than a planar fault by virtue of their contorted geometry. Distorted fault segments will then interact with adjacent ones and incorporate wall rocks into the CDZs with various structures. Also, the structural complexity can lead to co-existence of distributed shear in phyllosilicate, strain-hardening fault cores and localized shear in carbonate (Fig. 1b; Faulkner *et al.* 2003).

The 3-D seismic attribute method provides an effective tool to quantify the relative damage intensity in the subsurface and leads to the recognition of three CDZ types termed as the banded, box and dome CDZs (Figs 4e, g and i). We evaluate the evolution of these CDZ types by using the variance intensity as an indicator of the internal damage (Fig. 4a). We interpret the banded-CDZ (Figs 4d and e) to have formed via superposition of several subparallel faults with similar amount of slip and spaced at equal distance from one another. This evolution style fits the above mechanisms in which ancient fault cores are stronger than the surrounding rock bodies either during faulting (mechanism A) or by healing during 'quiescence'

(mechanism B) and the box-CDZ (Figs 4f and g) likely evolved by coalescence of multiple, closely spaced faults that linked separated fault segments that formed in earlier slip phases, in agreement with mechanism C. We interpret the dome-CDZ (Figs 4h and i) to have started as a banded-CDZ with multiple subparallel, strong faults, and during an advanced stage, one of the fault cores, in the centre or margins, became permanently weaker to accommodate later deformation by localized slip. This evolution fits the structural model of Aydin & Johnson (1978; Fig. 1a) in which after the development of multiple, closely spaced deformation-bands, each with ∼1 mm slip, a weak slip-surface with metres of slip develops at the margin of the damage zone. Our results illustrate complex but realistic spatial geometry of larger faults that could be renewed in future model simulations (e.g. UCERF3; Field *et al.* 2014).

4 CONCLUSIONS

Our data indicate that seismic attributes of curvature, variance and dip-azimuth may be used to characterize fault structure and related damage zones in the subsurface. The analysis of the Xujiahe sandstone reservoir in northeast Sichuan Basin revealed CDZs composed of multiple cores and damage zones with total width up to 1 km. Based on the damage distribution, we recognized three types of CDZs: the banded shape with a few clearly separated fault cores, the box shape with a few fault cores that coalesce with each other and dome shape with one dominant fault core and a few secondary ones. We infer that these CDZs evolved due to post-slip strengthening of the existing fault cores and geometric complexity of segmented fault zones. On the basis of this study, 3-D seismic attributes prove a valuable tool in illustrating the internal structure of CDZs in the subsurface.

ACKNOWLEDGEMENTS

Support funds (to ZL) were provided by Strategic Priority Research Program of the Chinese Academy of Sciences XDA14010306, the National Natural Science Foundation of China Nos. U1663203 and 41604036, and NSF grant (to ZR) EAR-1345087. ZL, WL, HZ, FH, KJM, and ZR analysed the results, ZL and ZR wrote the paper.

REFERENCES

Aydin, A. & Johnson, A.M., 1978. Development of faults as zones of deformation bands and as slip surfaces in sandstone, *Pure appl. Geophys.,* **116**(4–5), 931–942.

Badertscher, N.P. & Burkhard, M., 2000. Brittle-ductile deformation in the Glarus thrust Lochseiten (LK) calc-mylonite, *Terra Nova,* **12**(6), 281–288.

Ben-Zion, Y. & Andrews, D.J., 1998. Properties and implications of dynamic rupture along a material interface, *Bull. seism. Soc. Am.,* **88**(4), 1085–1094.

Ben-Zion, Y. & Sammis, C.G., 2003. Characterization of fault zones, *Pure appl. Geophys.,* **160**(3–4), 677–715.

Billi, A., Salvini, F. & Storti, F., 2003. The damage zone-fault core transition in carbonate rocks: implications for fault growth, structure and permeability, *J. Struct. Geol.,* **25,** 1779–1794.

Caine, J.S., Evans, J.P. & Forster, C.B., 1996. Fault zone architecture and permeability structure, *Geology,* **24**(11), 1025–1028.

Chester, F.M., Chester, J.S., Kirschner, D.L., Schulz, S.E. & Evans, J.P., 2004. Structure of large-displacement, strike-slip fault zones in the brittle continental crust, in *Rheology and Deformation in the Lithosphere at Continental Margins*, Vol. 1, pp. 223–260, eds Karner, G.D., Taylor, B., Driscoll, N.W. & Kohlstedt, D.L., Columbia University Press.

Chopra, S. & Marfurt, K.J., 2007. *Seismic Attributes for Prospect Identification and Reservoir Characterization,* SEG.

Di Toro, G. & Pennacchioni, G., 2005. Fault plane processes and mesoscopic structure of a strong-type seismogenic fault in tonalites (Adamello batholith, Southern Alps), *Tectonophysics,* **402**(1–4), 55–80.

Faulkner, D.R., Lewis, A.C. & Rutter, E.H., 2003. On the internal structure and mechanics of large strike-slip fault zones: field observations of the Carboneras fault in southeastern Spain, *Tectonophysics,* **367,** 235–251.

Faulkner, D.R., Jackson, C.A.L., Lunn, R.J., Schlische, R.W., Shipton, Z.K., Wibberley, C.A.J. & Withjack, M.O., 2010. A review of recent developments concerning the structure, mechanics and fluid flow properties of fault zones, *J. Struct. Geol.,* **32**(11), 1557–1575.

Field, E.H. *et al.*, 2014. Uniform California Earthquake Rupture Forecast, Version 3 (UCERF3)—the time-independent model, *Bull. seism. Soc. Am.,* **104**(3), 1122–1180.

Heesakkers, V., Murphy, S., Lockner, D.A. & Reches, Z., 2011. Earthquake rupture at focal depth, Part II: Mechanics of the 2004 M2.2 earthquake along the Pretorius Fault, TauTona Mine, South Africa, *Pure appl. Geophys.,* **168**(12), 2427–2449.

Iacopini, D. & Butler, R.W., 2011. Imaging deformation in submarine thrust belts using seismic attributes, *Earth planet. Sci. Lett.,* **302**(3–4), 414–422.

Johansen, T.E.S., Fossen, H. & Kluge, R., 2005. The impact of syn-faulting porosity reduction on damage zone architecture in porous sandstone: an outcrop example from the Moab Fault, Utah, *J. Struct. Geol.,* **27**(8), 1469–1485.

Li, J., Hu, D., Zou, H., Shang, X., Ren, H. & Wang, L., 2016. Coupling relationship between reservoir diagenesis and gas accumulation in Xujiahe Formation of Yuanba–Tongnanba area, Sichuan Basin, China, *J. Nat. Gas Geosci.,* **1**(5), 335–352.

Liao, Z., Liu, H., Carpenter, B.M., Marfurt, K.J. & Reches, Z.E., 2018. Analysis of fault damage–zones using 3D seismic coherence in the Anadarko Basin, Oklahoma, *AAPG Bull.,* **103**(8), 1771–1785.

Liao, Z., Weilun, C., Xiaofeng, C., Huayao, Z. & Hao, F., 2020. Multi-scale fracture and damage zone characterization in a tight sandstone reservoir, Sichuan Basin, China, *Interpretation* **8** (4), 1–17.

Lockner, D.A., Morrow, C., Moore, D. & Hickman, S., 2011. Low strength of deep San Andreas fault gouge from SAFOD core, *Nature,* **472,** 82–85.

Lyakhovsky, V. & Ben-Zion, Y., 2009. Evolving geometrical and material properties of fault zones in a damage rheology model, *Geochem. Geophys. Geosyst.,* **10**(Q11011), doi:10.1029/2009GC002543.

Marfurt, K.J., 2006. Robust estimates of 3D reflector dip and azimuth, *Geophysics,* **71**(4), 29–40.

Mitchell, T.M. & Faulkner, D.R., 2009. The nature and origin of off-fault damage surrounding strike-slip fault zones with a wide range of displacements: a field study from the Atacama fault system, northern Chile, *J. Struct. Geol.,* **31**(8), 802–816.

Muhuri, S.K., Dewers, T.A., Scott, T.E., Jr. & Reches, Z., 2003. Interseismic fault strengthening and earthquake-slip instability: friction or cohesion? *Geology,* **31,** 881–884.

Peng, Z., Ben-Zion, Y., Michael, A.J. & Zhu, L., 2003. Quantitative analysis of seismic fault zone waves in the rupture zone of the 1992 Landers, California, earthquake: evidence for a shallow trapping structure, *Geophys. J. Int.,* **155**(3), 1021–1041.

Powers, P.M. & Jordan, T.H., 2010. Distribution of seismicity across strike-slip faults in California, *J. geophys. Res.,* **115**(B05305), doi:10.1029/2008JB006234.

Reches, Z. & Lockner, D., 1994. Nucleation and growth of faults in brittle rocks, *J. geophys. Res.,* **99**(B9), 18 159–18 173.

Sagy, A., Reches, Z.E. & Roman, I., 2001. Dynamic fracturing: field and experimental observations, *J. Struct. Geol.,* **23**(8), 1223–1239 .

Savage, H.M. & Brodsky, E.E., 2011. Collateral damage: evolution with displacement of fracture distribution and secondary fault strands in fault damage zones, *J. geophys. Res.,* **116**(B3), 428–452.

Scholz, C.H., 2002. *The Mechanics of Earthquakes and Faulting,* Vol. 471, Cambridge Univ. Press.

Teng, F.Y., 2005. The Study of Mountainous Region 3D Seismic Survey, *Thesis*, China University of Petroleum-Huadong, Dongying, Shandong, China.

Valoroso, L., Chiaraluce, L. & Collettini, C., 2014. Earthquakes and fault zone structure, *Geology,* **42**(4), 343–346.